ISBN: 978-3-95450-260-8 ISSN: 2673-5547 doi: 10.18429/JACoW-HIAT2025-TUB01

A SINGLE-SLICE ROTATING GRAPHITE TARGET AT FRIB*

J. Song†, N. Bultman, D. Cole, N. Jockheck, T. Kanemura, M. Larmann, D. Lee, G. Lee, S. Miller, M. Patil, M. Portillo, R. Quispe-Abad, M. Reaume, J. Simon, M. Steiner, J. Wei
Facility for Rare Isotope Beams, Michigan State University, East Lansing, MI, USA

Abstract

The FRIB accelerator, constructed and commissioned in 2022, serves as a leading facility for producing rare isotope beams and exploring elements beyond the limits of stability. These beams are produced by reactions between stable primary beams and a graphite production target. Meanwhile, approximately 20–40% of the primary beam power is deposited in the target, necessitating efficient heat dissipation. Currently, FRIB operates at a primary beam power of 20 kW. To enhance thermal dissipation efficiency, a single-slice rotating graphite target with a diameter of approximately 30 cm is employed. This paper presents an overview of the current status of the production target system and ongoing R&D efforts to enhance its performance and durability under high-power beam conditions.

INTRODUCTION

The Facility for Rare Isotope Beams (FRIB), a leading facility for rare isotope science, is undergoing a staged power ramp-up toward its ultimate goal of operating at 400 kW of primary beam power. FRIB currently delivers high-intensity stable ion beams ranging from oxygen to uranium and has been progressively increasing its operational beam power from 1 kW to 20 kW [1, 2] since commissioning in 2022 [3, 4]. This capability enables a wide range of nuclear science experiments, including studies of nuclear structure, reactions, and astrophysical processes. To address the intense thermal loads associated with rare isotope production, FRIB employs a single-slice rotating graphite target system [5]. This target is designed to withstand beam powers up to 50 kW, with thermal mitigation achieved by distributing the deposited energy over a larger surface area through disc rotation. This reduces surface power density and enhances thermal performance. The current system utilizes a disc approximately 30 cm in diameter, operating at moderate rotational speeds (500 rpm). The rotation speed is planned to increase to 2000 rpm in future operation to reduce both the peak temperature and the temperature gradient across the irradiated beam spot on the graphite disc. In addition to thermal and mechanical factors, radiation-induced degradation strongly influences the operational durability of the target. Radiation transport simulations indicate that radiation damage to the graphite remains relatively low on the order of 0.4 displacements per atom (DPA) even under worst-case uranium irradiation scenarios. This low damage level allows for multiple reuses of a single disc, with the operational plan calling for retirement after approximately ten irradiation cycles. The structural configuration of the target assembly is illustrated in Fig. 1. Since the initial operation in 2022, several key hardware improvements have been implemented, including the adoption of high-temperature bearings and the application of a high-emissivity internal coating ($\epsilon \approx 0.9$) to enhance radiative heat transfer.

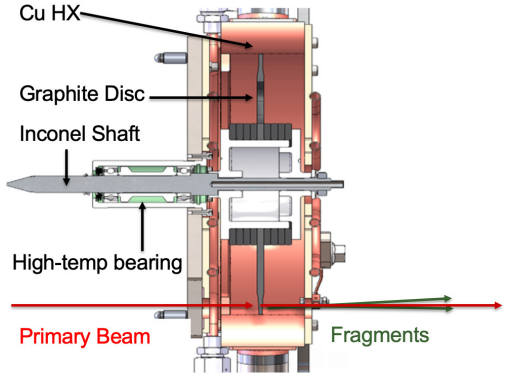

Figure 1: FRIB target assembly.

PRODUCTION TARGET

The production target system illustrated in Fig. 1 consists of a 30 cm diameter graphite disc (Mersen grade 2360), spacers made of the same graphite grade, a YSZ ceramic hub, high-temperature bearings (NSK), an Inconel shaft, and a copper heat exchanger. The interior surface of the heat exchanger was coated with a high-emissivity paint (Aremco 840-MS). Between 20–40 % of the primary beam power is deposited in production targets of varying thickness. The primary cooling mechanism is radiative heat transfer from the rotating graphite disc, with the emitted heat absorbed by side-mounted heat exchangers and water-cooled front and rear doors.

To accommodate various primary beams, eight production targets with different thicknesses are provided to optimize secondary beam yields. The configurations are summarized in Table 1. To achieve efficient secondary beam delivery, the most critical requirement is to maintain the target defect within ±2 %, which accounts for machining tolerances, material inhomogeneities, and mechanical deformations. Recent measurements using a wedge view with beam data from ARIS indicate that the total defect is approximately 1.6 % [6]. To support consistent quality in spare targets, a system [7] capable of directly measuring the physical thickness has been developed, it was confirmed that for targets with thicknesses ranging from 2.1 mm to 5 mm, the machining precision

* Work supported by the U.S. Department of Energy Office of Science under Cooperative Agreement DE-SC0023633, the State of Michigan, and Michigan State University.
† songj@frib.msu.edu

ISBN: 978-3-95450-260-8 ISSN: 2673-5547 doi: 10.18429/JACoW-HIAT2025-TUB01

Table 1: Summary of Graphite Target Thicknesses, Corresponding Areal Densities, and Associated Primary Beams Used in Operation

Target thick. (mm)	Areal density (g/cm^2)	Primary Beam
1.2	0.23	^{238}U
2.1	0.39	^{124}Xe, ^{198}Pt, ^{238}U
3.5	0.65	^{124}Xe, ^{92}Mo
5.0	0.95	^{48}Ca, ^{58}Ni
8.0	1.54	^{18}O, ^{48}Ca, ^{70}Ge, ^{82}Se
10.0	1.86	^{40}Ar, ^{48}Ca
15.0	2.79	-
18.0	3.35	^{28}Si

results in thickness variations that are, at minimum, within ≈ 1 % at the 2σ confidence level. Accurate implementation of temperature-dependent material properties and thermal contact conductance (TCC) is essential for reliable thermal simulations, as well as for establishing beam power limits and ensuring safe operating conditions. Surface emissivities of key components in the target system, including the graphite disc, high-emissivity–coated copper heat exchanger, Inconel shaft, and aluminum wing, were measured using the custom-built setup [8]. The measured emissivity values as a function of temperature are presented in Fig. 2. In addition, the TCCs for the spindle assembly were evaluated using the dedicated vacuum-based measurement system [9].

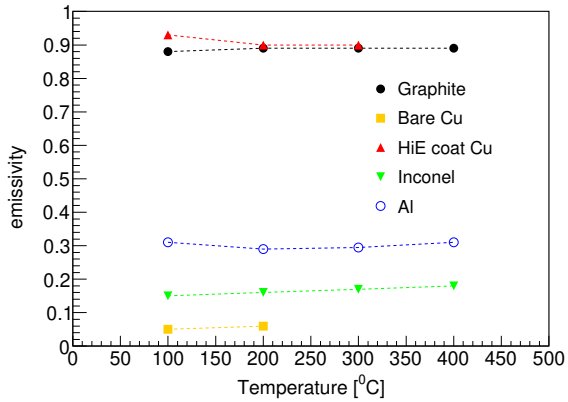

Figure 2: Surface emissivity measurements of target system materials, graphite, bare copper, high emissivity coated copper, Inconel, and aluminum, are shown as a function of temperature.

THERMAL BEHAVIOR OF THE PRODUCTION TARGET

Approximately 20–40 % of the primary beam power is deposited in the target, delivered by a Gaussian beam with a 1σ beam size of 0.25 mm, regardless of the primary beam species. For the thermal analysis based on the deposited power, the entire target assembly was modeled using ANSYS [10]. In the simulation, surface emissivities and the TCC for the spindle were taken from our measurements. Other physical properties, such as thermal conductivity, were adopted from known reference values. The TCC for the graphite was estimated based on literature data [11]. A validation test of the TCC using the full disc module assembly is planned, and the validated values will be incorporated into the thermal analysis model. The majority of the heat is absorbed by the graphite disc, which subsequently radiates to the heat exchanger. The exchanger removes over 99 % of the deposited power via water cooling through the front and rear doors and the side section. Only a small fraction (<1 %) is conducted into the spindle; however, even this small amount of power can raise the bearing temperature beyond its operational limit.

To validate our thermal analysis of the graphite target, we compared the maximum temperature on the 8 mm-thick rotating graphite disc as measured by a thermal imaging system (TIS) [12, 13], at various levels of deposited power. The maximum temperatures resulting from irradiation with ^{48}Ca and ^{82}Se beams on an 8 mm-thick graphite disc rotating at 500 rpm were recorded during beam operations over the past two years, with primary beam powers ranging from 5 to 20 kW. Representative thermal images at $\approx$ 20 kW are shown in the top panels of Fig. 3. In the images, the disc rotates counterclockwise, as evidenced by the trailing edge of the beam spot. The observed maximum temperatures for ^{48}Ca and ^{82}Se beams were 917°C and 1146°C, respectively. These measurements are subject to a few percent uncertainty due to variations in emissivity, calibration accuracy, and beam current fluctuations. Measured and simulated maximum temperatures as a function of deposited beam power are compared in Fig. 3, using 13 recorded data points. Since the front door of the heat exchanger is only partially coated ($\approx$ 1/4 remains coated), thermal simulations were conducted for two boundary conditions: fully coated and uncoated. In the model, beam power was deposited uniformly across the graphite disc thickness. The comparison between measured and simulated maximum temperatures shows good agreement within 4 %.

BEAM POWER CONSTRAINTS

Beam power constraints are determined based on the thermal limits of key components in the target system. These include the maximum allowable temperatures for the graphite disc (<1900°C), target bearing (<250°C), Inconel shaft (<650°C), and ceramic hub (<1000°C). Thermal simulations and operational planning ensure that all components remain within these limits under specified beam power conditions. Based on thermal simulation results using the complete target assembly model, beam power constraints were evaluated for both the most frequently used 2.1 mm and 8.0 mm-thick graphite discs. For both 2.1 mm and 8.0 mm-thick graphite discs, the predicted maximum temperature are shown in Fig. 4 a), and the corresponding maximum allowable deposited powers as a function of rotational speed are presented in Fig. 4 b). The temperature limits of other com-

ISBN: 978-3-95450-260-8 ISSN: 2673-5547 doi: 10.18429/JACoW-HIAT2025-TUB01

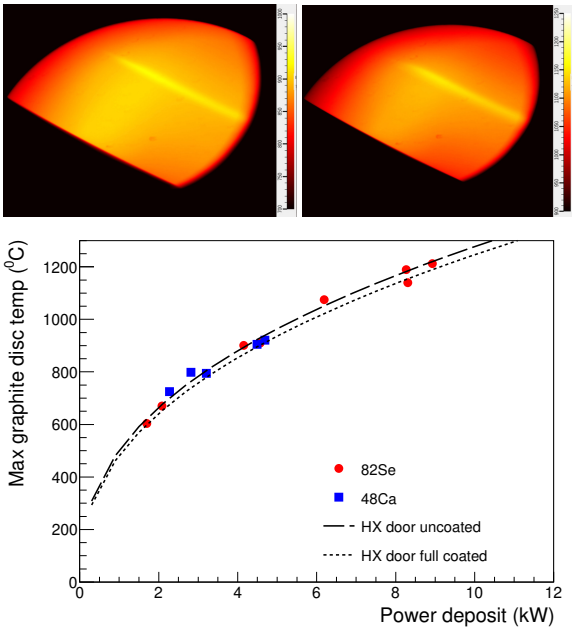

Figure 3: Thermal images for a 19 kW, 215 MeV/u ^{48}Ca beam (top left) and a 20 kW, 225 MeV/u ^{82}Se beam (top right) incident on a rotating graphite disc. Bottom: Comparison between measured and simulated maximum temperatures of the graphite disc as a function of deposited beam power for ^{48}Ca (blue squares) beams and ^{82}Se (red circles). The data correspond to an 8 mm-thick graphite disc rotating at 500 rpm. Simulated results are shown for two thermal boundary conditions at the heat exchanger: uncoated (solid line) and fully coated with a high-emissivity surface (dashed line).

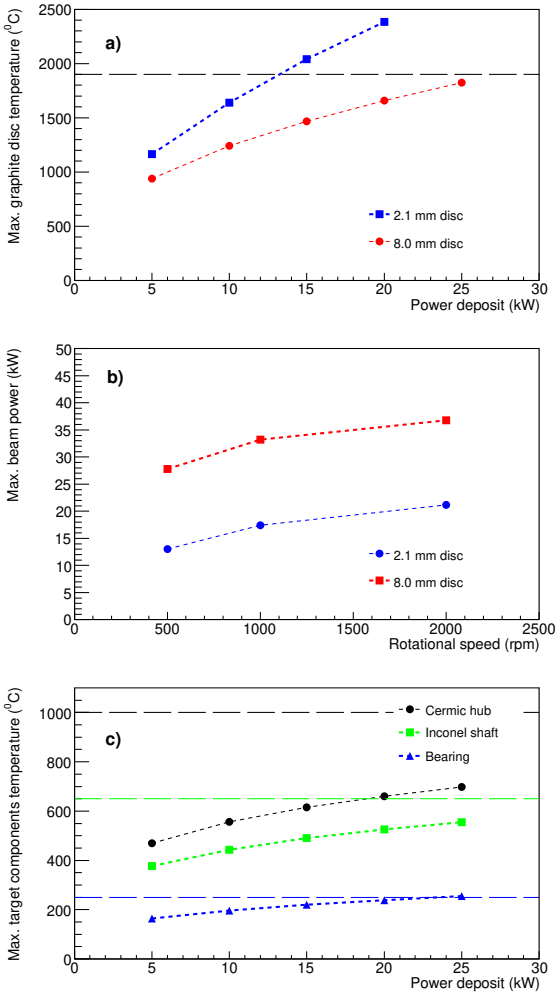

Figure 4: a) Simulated maximum temperature of graphite discs as a function of deposited power for 2.1 mm and 8.0 mm-thick targets. The dashed horizontal line indicates the graphite temperature limit of 1900°C. b) Maximum allowable deposited beam power into the target as a function of rotational speed for both disc thicknesses. c) Simulated maximum temperatures of other critical components, ceramic hub, Inconel shaft, and bearing, as a function of deposited power, along with their respective temperature limits (dashed lines).

ponents are primarily proportional to the deposited power in the target, with negligible dependence on target thickness and rotational speed. The maximum temperatures of each component as a function of deposited power are illustrated in Fig. 4 c). Operation appears feasible up to ≈ 25 kW of deposited power. As examples, for a 177 MeV/u ^{238}U beam incident on a 2.1 mm-thick target, operation is feasible with upto 21 kW of deposited power (equivalent to 57 kW of primary beam power) at a rotational speed of 2000 rpm. Similarly, for a 225 MeV/u ^{82}Se beam on an 8 mm-thick target, upto 37 kW of deposited power (equivalent to 88 kW of primary beam power) can be accommodated at 2000 rpm.

CONCLUSION

The single-slice rotating graphite target system at FRIB has demonstrated stable and reliable performance under primary beam powers of up to 20 kW. Design improvements such as the integration of high-temperature bearings, application of high-emissivity coatings inside heat exchanger have significantly improved thermal performance of the system. Comprehensive R&D activities have supported the development and validation of a predictive thermal model. These efforts include experimental measurements of key thermal properties such as surface emissivity and the TCC, and validation of simulated temperatures using beam-induced thermal imaging data. The comparison between measurements and simulations shows agreement within 4 %, supporting the accuracy of the model. Thermal simulations further demonstrate that all critical components including the graphite disc, Inconel shaft, ceramic hub, and bearings, remain within safe temperature limits for both 2.1 mm and 8.0 mm-thick targets, operated at 2000 rpm and 1000 rpm, respectively, for primary beam powers up to at least 50 kW. These results confirm that the current system configuration is suitable for continued operation during the transitional power ramp-up phase.

ISBN: 978-3-95450-260-8 ISSN: 2673-5547 doi: 10.18429/JACoW-HIAT2025-TUB01

REFERENCES

[1] J. Wei *et al.*, "Technological developments and accelerator improvements for the FRIB beam power ramp-up", *J. Instrum.*, vol. 19, no. 05, p. T05011, May 2024. doi:10.1088/1748-0221/19/05/t05011

[2] P. N. Ostroumov *et al.*, "Acceleration of uranium beam to record power of 10.4 kW and observation of new isotopes at Facility for Rare Isotope Beams", *Phys. Rev. Accel. Beams*, vol. 27, no. 6, p. 060101, Jun. 2024. doi:10.1103/physrevaccelbeams.27.060101

[3] J. Wei *et al.*, "Accelerator commissioning and rare isotope identification at the Facility for Rare Isotope Beams", *Mod. Phys. Lett. A*, vol. 37, no. 09, p. 2230006, Mar. 2022. doi:10.1142/s0217732322300063

[4] M. Portillo *et al.*, "Commissioning of the Advanced Rare Isotope Separator ARIS at FRIB", *Nucl. Instrum. Methods Phys. Res., Sect. B*, vol. 540, pp. 151–157, Jul. 2023. doi:10.1016/j.nimb.2023.04.025

[5] F. Pellemoine *et al.*, "Thermo-mechanical behaviour of a single slice test device for the FRIB high power target", *Nucl. Instrum. Methods Phys. Res., Sect. A*, vol. 655, no. 1, pp. 3–9, Nov. 2011. doi:10.1016/j.nima.2011.06.010

[6] M. Portillo and M. Steiner, private communication.

[7] D. Lee *et al.*, "Physical Thickness Characterization of the FRIB Production Targets", unpublished.

[8] S. Yoon *et al.*, "Emissivities of the FRIB Production Target Components", unpublished.

[9] G. Lee *et al.*, "Thermal simulation validation for the rotating single-slice graphite target system", unpublished.

[10] M. Patil, J. Song, M. Reaume, M. Larmann, N. Bultman, and R. Quispe-Abad, "Thermal analysis of rotating single slice graphite target system for FRIB", in *Proc. IPAC'24*, Nashville, TN, USA, May 2024, pp. 3827–3829. doi:10.18429/JACoW-IPAC2024-THPS41

[11] K. Ioki, M. Nishikawa, I. Tatsumi, T. Uchikawa, and M. Fujiwara, "Measurement of Contact Resistance and Heat Load Test on Graphite Limiter", *J. Nucl. Sci. Technol.*, vol. 22, no. 7, pp. 529–537, Jul. 1985. doi:10.1080/18811248.1985.9735694

[12] I. N. Nesterenko, G. Bollen, M. Hausmann, A. Hussain, S. M. Lidia, and S. Rodriguez Esparza, "Optical System for Observation of FRIB Target", in *Proc. NAPAC'19*, Lansing, MI, USA, Sep. 2019, pp. 570–572. doi:10.18429/JACoW-NAPAC2019-TUPLE05

[13] D. McNanney, S. Cogan, I. Nesterenko, S. Lidia, J. Song, and E. Daykin, "FRIB target thermal image processing for accurate temperature mapping", in *Proc. IPAC'24*, Nashville, TN, USA, May 2024, pp. 3409–3412. doi:10.18429/JACoW-IPAC2024-THPG62